Chirality dependence of coherent phonon amplitudes in single-wall carbon nanotubes

A. R. T. Nugraha, G. D. Sanders, K. Sato, C. J. Stanton, M. S. Dresselhaus, and R. Saito

Phys. Rev. B **84**, 174302 — Published 11 November 2011

DOI: 10.1103/PhysRevB.84.174302

Chirality dependence of coherent phonon amplitudes in single wall carbon nanotubes

A. R. T. Nugraha[1], G. D. Sanders[2], K. Sato[1], C. J. Stanton[2], M. S. Dresselhaus[3], R. Saito[1]
[1]*Department of Physics, Tohoku University, Sendai 980-8578, Japan*
[2]*Department of Physics, University of Florida, Box 118440, Gainesville, Florida 32611-8440, USA*
[3]*Department of Physics, Massachusetts Institute of Technology, Cambridge, MA 02139-4307, USA*
(Dated: October 18, 2011)

We simulate the ultrafast dynamics of laser-induced coherent phonons in single wall carbon nanotubes (SWNTs). In particular, we examine the radial breathing mode (RBM) coherent phonon amplitude as a function of excitation energy and chirality. We find that the RBM coherent phonon amplitudes are very sensitive to changes in excitation energy and are strongly chirality dependent. We discuss how the SWNT diameter changes in response to femtosecond laser excitation and under what conditions the diameter of a given SWNT will initially increase or decrease. An effective-mass theory for the electron-phonon interaction gives a physical explanation for these phenomena.

PACS numbers: 78.67.Ch,78.47.J-,63.20.kd

I. INTRODUCTION

Single wall carbon nanotubes (SWNTs), with their unique physical properties, have been an exciting material for study.[1–5] In particular, SWNTs provide a one-dimensional (1D) model system for studying the dynamics and interactions of electrons and phonons, which strongly depend on the SWNT geometrical structure as characterized by their chiral indices (n, m).[1] With rapid advances in ultrafast pump-probe spectroscopy, it is now possible to monitor photoexcited SWNT coherent phonon lattice vibrations in real time.[6–10]

In pump-probe spectroscopy, femtosecond laser pump pulses rapidly generate photoexcited electron-hole pairs (excitons) in the excited states of the SWNT sample. The electron-hole pairs couple to phonons causing the SWNT lattice to vibrate. The vibrations are coherently driven by electron-phonon (or more precisely exciton-phonon) interactions.[11] The coherent phonon vibrations are observed as oscillations in either the differential transmission or differential reflectivity ($\Delta T/T$ or $\Delta R/R$) in the delayed probe pulse as a function of the probe delay time. After Fourier transformating $\Delta T/T$ or $\Delta R/R$ with respect to time, we obtain the coherent phonon spectra as a function of phonon frequency. Several peaks found in the coherent phonon spectra correspond to specific coherent phonon modes. Typical SWNT phonon modes observed in coherent phonon spectra are similar to those found in Raman spectra since the electron-phonon interaction plays a role in both coherent phonon excitation and Raman spectroscopy. For example, using coherent phonon spectroscopy we can observe both the radial breathing mode (RBM) and the G mode which have also been seen in Raman spectroscopy.[6–8]

Recent experiments have given us some hints that the coherent phonon intensity for a particular SWNT strongly depends on the excitation energy, although a systematic behavior related to the SWNT types is not yet well-understood.[9,12] In a previous study, Sanders *et al.*[13] calculated coherent phonon intensities for the RBM phonons of two nanotube families, namely the type-I ($\mathrm{mod}(2n + m, 3) = 1$) and the type-II ($\mathrm{mod}(2n + m, 3) = 2$) semiconducting SWNTs, and found that the coherent phonon intensity in type-I nanotubes was generally larger than that in type-II nanotubes. However, the results were limited to a small number of SWNT chiralities. It is thus necessary to verify the trends by examining more SWNT species. A detailed physical reason for the chirality-dependent coherent phonon intensity is also missing. Moreover, it was recently noticed that some SWNTs start their coherent RBM vibrations by initially expanding their diameters, while others start their RBM vibrations by initially shrinking their diameters.[12,14] Since this phenomenon depends on the nanotube types, it is important to examine the k-dependent electron-phonon interaction. We take this issue as the main focus of the present paper.

We focus on the coherent phonon *amplitude* instead of its intensity because the amplitude can give phase information that is not obtainable from the intensity. For instance, from the amplitude we can tell whether the diameter of a specific SWNT in the coherent RBM will initially expand or contract at a given excitation energy. In Sec. II, we explain the method adopted to calculate the coherent phonon amplitudes, where we have used and modified a computer package developed in a previous study by Sanders *et al.*[13] Here we mainly study the $(11, 0)$ and $(13, 0)$ semiconducting zigzag nanotubes as examples for discussing the excitation and chirality dependence of the RBM coherent phonon amplitudes. We note that the electron-phonon interaction plays an important role in determining the phase or sign of the RBM coherent phonon diameter oscillations, and hence determines whether the SWNT diameter initially expands or contracts. This discussion is covered in Sec. III, in which the RBM electron-phonon interaction in SWNTs is derived in an effective-mass theory. Though the main examples studied in this work are semiconducting SWNTs, the theory is also valid for metallic SWNTs[15], since it is shown in Sec. IV that the chirality dependence of the coherent phonon amplitude between different nanotube types has the same origin. As a guide for experimentalists, in Sec. IV

we also present the RBM coherent phonon amplitudes for 31 SWNTs with diameters in the range of $0.7 - 1.1\,\mathrm{nm}$. The RBM coherent phonon amplitudes are mapped as a function of (n, m) for optical transition energies E_{11} or E_{22} found within $1.5 - 3.0\,\mathrm{eV}$, where i in E_{ii} denotes the optical transitions between the i-th valence and i-th conduction subbands.[16] Mapping the coherent phonon amplitudes and initial phases as a function of tube diameter should be a useful guide for predicting the initial direction of the SWNT coherent RBM lattice vibrations. A summary and perspectives for future research are given in Sec. V.

II. COHERENT PHONON AMPLITUDES

A. Calculation method

To calculate the SWNT coherent phonon amplitudes, we use a computer program developed in previous work,[13] which obtains coherent phonon amplitudes by solving a driven harmonic oscillator equation derived from the Heisenberg equations of motion.[17] In this program, we incorporate SWNT electronic energies and wave functions obtained from an extended tight-binding (ETB) calculation,[18] the phonon-dispersion relations and corresponding phonon modes,[19] the electron-phonon interaction matrix elements,[20] the optical matrix elements,[21] and the interaction of carriers with an ultrafast laser pulse.

As noted in Sanders *et al.*[13], only $q = 0$ phonon modes are coherently excited if the pump laser spot size is large compared with the size of the nanotube. For coherent phonons to be excited, it is necessary for the pump pulse to have a duration shorter than the phonon period (so that the pump pulse power spectrum has a Fourier component at the phonon frequency). In a simple forced oscillator model neglecting oscillation decays, the coherent RBM phonon amplitude Q with frequency ω satisfies a driven oscillator equation,[13]

$$\frac{\partial^2 Q(t)}{\partial t^2} + \omega^2 Q(t) = S(t), \tag{1}$$

subject to the initial conditions $Q(0) = 0$ and $\dot{Q}(0) = 0$. Here $S(t)$ is the driving function which depends on the photoexcited carrier distribution function and is given by[13]

$$S(t) = -\frac{2\omega}{\hbar} \sum_{\mu k} M^{\mu}_{\mathrm{el-ph}}(k)\ \delta f^{\mu}(k, t), \tag{2}$$

where $M^{\mu}_{\mathrm{el-ph}}(k)$ is the k-dependent RBM electron-phonon matrix element for the μ-th cutting line (1D Brillouin zone of a SWNT)[1,22,23] and δf^{μ} is the net photogenerated electron distribution function with a pump pulse pumping at the E_{ii} transition energy as obtained by solving a Boltzmann equation for the photogeneration process. The photogeneration rate in the Boltzmann equation depends on the excitation laser energy[13] and it also contains the electron-photon matrix element M_{op} for the case of light polarized along the tube axis, so that we have the proportionality

$$\delta f^{\mu} \propto M^{\mu}_{\mathrm{op}}. \tag{3}$$

In a typical calculation, the necessary inputs are the excitation energy, E_{laser} and the chiral index (n, m). For a given excitation energy, we solve Eq. (1) for a specific SWNT to obtain the coherent RBM phonon amplitude oscillating at the RBM frequency. Unless otherwise mentioned, we use the same common input parameters for the pump-probe setup as those used in Ref. 8, *i.e.*, we excite the RBM phonons with a single 50 fs laser pulse, where the pump fluence is taken to be 10^{-5} J/cm^2, and the FWHM spectral linewidth is assumed to be $0.15\,\mathrm{eV}$. Here we do not have to consider excitonic effects because we will not discuss the peak positions or line shapes of the coherent phonon spectra. For such discussions, the excitonic effects cannot be neglected since the E_{ii} energies are shifted from those calculated within a single particle picture[11,24]. In the present paper, however, we can plot $M^{\mu}_{\mathrm{el-ph}}(k)$ as a function of k and show that our treatment is reasonable. Considering only the electron-phonon interaction instead of the exciton-phonon interaction is acceptable because the exciton size in k-space is much smaller than the width of the electron-phonon matrix elements. For example, based on a calculation from our exciton program,[24] the exciton size in k space for the $(11, 0)$ nanotube at the E_{22} transition is about $0.043\ \pi/T$, while the width of the electron-phonon matrix element at the same energy is about $0.4\ \pi/T$ where T is the unit cell length. The exciton size in k space is only about 10% of the width of the electron-phonon interaction. The exciton-phonon interaction is given by integrating $M^{\mu}_{\mathrm{el-ph}}(k)$ in k-space weighted by the exciton wavefunction.[25] Therefore, the electron-phonon interaction is approximately constant as a function of 1D k for this small k region, *i.e.* the size of the exciton wavefunction. In fact, the value of the exciton-phonon interaction is on the same order as the electron-phonon interaction.[25]

B. Calculation results

In Fig. 1, we plot the coherent RBM phonon amplitude $Q_{\rm m}$ in an $(11,0)$ nanotube at an early time, along with the absorption coefficient as a function of $E_{\rm laser}$. Here $Q_{\rm m}$ can be imagined by roughly defining $Q(t) = Q_{\rm m}\cos\omega t$, where the origin of time is now indicated by the first maximum (minimum) of $Q(t)$ found after $t = 0$ for a positive (negative) coherent phonon vibration. Therefore, in this definition, $Q_{\rm m} > 0$ and $Q_{\rm m} < 0$ correspond to the tube diameter expansion and contraction, respectively (cf. Q(t) plots in Ref. 13). From Fig. 1, we see that the pump light is strongly absorbed at the E_{ii} energies. The resulting increase in the number of photoexcited carriers increases the coherent phonon driving function $S(t)$ in Eq. (2) and thus enhances the coherent phonon oscillation amplitude near the E_{ii} transitions. Note that at E_{11} the amplitude has a negative sign, indicating that the tube diameter initially shrinks and oscillates about a smaller diameter, while at E_{22} and higher energies (e.g., E_{33} or E_{44}) the tube diameter initially expands and oscillates about a larger diameter. According to a common concept based on the Franck-Condon principle, solid lattices usually tend to expand in the presence of ultrafast carrier photoexcitation since the electronic excited states are anti-bonding states. When an electron is excited, it will try to find a new equilibrium position at the minimum of the excited anti-bonding state energy. This minimum energy is located at a larger coordinate than that of the ground state, and thus the lattice expands. However, this is not always the case for RBM coherent phonons in the SWNT system, where the tube diameter can either expand or contract depending on the excitation energy.

In order to understand this phenomenon, we consider the magnitude and phase of the oscillation amplitude $Q(t)$ driven by $S(t)$ in Eq. (2). First, since $\delta f \propto M_{\rm op}$ as in Eq. (3), the magnitude of oscillations should be proportional to the product of the electron-phonon and electron-photon matrix elements:

$$|Q| \propto |M_{\rm el-ph}||M_{\rm op}|. \tag{4}$$

Second, according to Eq. (2) and noting that $\delta f^{\mu}(k)$ is usually positive for most cases of interest (*i.e.* no gain in the system), the initial phase of $Q(t)$ is only determined by the sign of $M^{\mu}_{\rm el-ph}(k)$ summed over all cutting lines μ and all k points. The unique values of $|M_{\rm el-ph}|$ and $|M_{\rm op}|$ for a fixed selection of energy and (n,m) then determines the excitation energy and chirality dependence of the coherent phonon amplitudes.

Let us discuss the type dependence of coherent RBM phonon amplitudes by comparing two semiconducting zigzag nanotubes of different families and types. In Fig. 2, we plot the electron-phonon matrix elements for RBM coherent phonons in the $(11,0)$ (type-I) and $(13,0)$ (type-II) nanotubes as a function of 1D wavevector k. The k dependence of $M^{\mu}_{\rm el-ph}(k)$ for the RBM phonon is shown for the first two cutting lines, for E_{11} and E_{22}. As can be seen in the figure, both positive and negative values of $M^{\mu}_{\rm el-ph}(k)$ are possible. Also, according to Eq. (2), if we pump near the E_{ii} band edge, the electron distributions would be localized near $k = 0$ in the 1D Brillouin zone of the zigzag nanotubes, for which the k_{ii} points for the E_{ii} energies lie at $k = 0$. Therefore, the positive (negative) values of $S(t)$ at the E_{22} (E_{11}) transition energy are determined by the negative (positive) value of $M^{\mu}_{\rm el-ph}(k)$ near $k = 0$. For the two nanotubes, the signs of the electron-phonon matrix elements differ at E_{11} and E_{22}. The reason is that for type-I and type-II nanotubes the E_{11} and E_{22} cutting line positions with respect to the K-point in the 2D graphene Brillouin

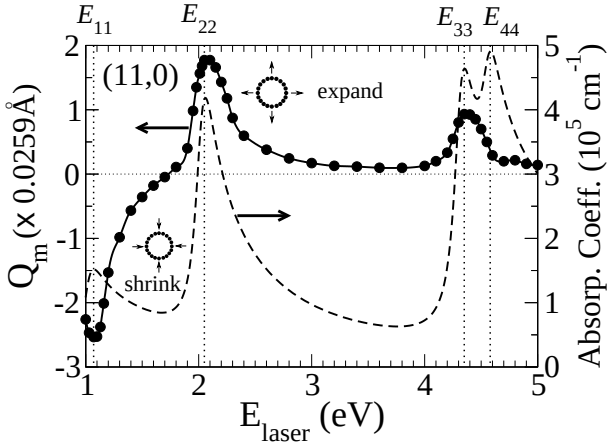

FIG. 1: The coherent RBM phonon amplitude $Q_{\rm m}$ for an $(11,0)$ zigzag tube as a function of laser excitation energy $E_{\rm laser}$. For clarity, $Q_{\rm m}$ is plotted in units of 0.0259 Å. A positive (negative) sign of the vibration amplitude denotes a vibration whose initial phase corresponds to an expanding (shrinking) diameter. The absorption coefficient versus $E_{\rm laser}$ is shown for comparison with the $Q_{\rm m}$ behavior.

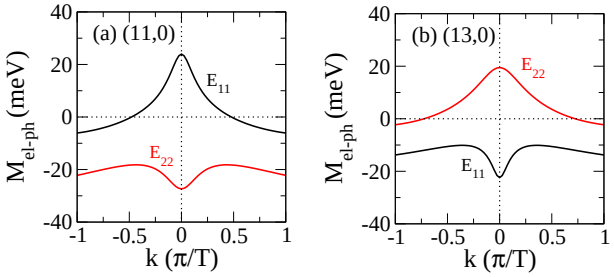

FIG. 2: (Color online) RBM electron-phonon matrix elements of (a) $(11,0)$ and (b) $(13,0)$ zigzag nanotubes within the ETB approximation.

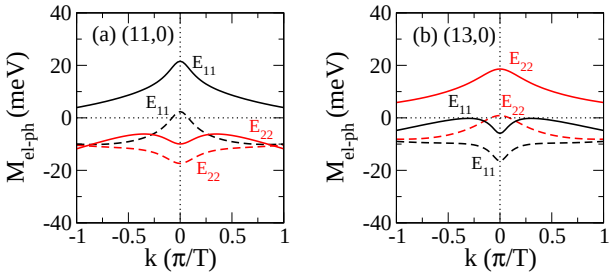

FIG. 3: (Color online) Electron and hole components of the ETB $M_{\mathrm{el-ph}}$ shown by solid and dashed lines, respectively, for (a) $(11,0)$ and (b) $(13,0)$ zigzag nanotubes, as a function of k. The matrix elements for E_{11} and E_{22} are shown in black and red, respectively.

zone are opposite to each other.[22] Depending on the cutting line positions relative to the K-point, the corresponding $M^{\mu}_{\mathrm{el-ph}}(k)$ for a given cutting line is negative in the region to the right of the K-point and positive in the region to the left.[26] This will be proved in the next section using an effective-mass theory developed by Sasaki *et al.*[27] From this argument, we predict that the type-I (type-II) zigzag nanotubes would start their coherent RBM phonon oscillations by initially decreasing (increasing) the tube diameter at E_{11}, while at E_{22} the behavior is just the opposite, as shown in Fig. 2.

III. ANALYSIS OF THE ELECTRON-PHONON INTERACTION

Since the electron-phonon matrix element determines the initial lattice response of the SWNTs, we further decompose $M_{\mathrm{el-ph}}$ into its electron and hole components for each SWNT in order to understand which component gives a significant contribution to the ETB matrix element $M_{\mathrm{el-ph}}$. This electron-phonon matrix element for the photo-

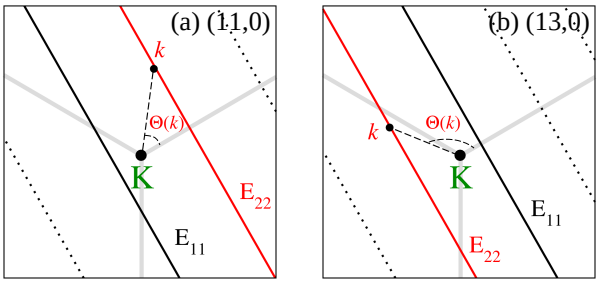

FIG. 4: (Color online) Cutting lines for (a) (11,0) and (b) (13,0) zigzag nanotubes near the graphene K-point. Black and red solid lines denote the E_{11} and E_{22} cutting lines, respectively, while the dotted lines correspond to higher cutting lines. The angle $\Theta(\boldsymbol{k})$ is measured counterclockwise from a line perpendicular to the cutting lines, where the positive direction of the line is to the right of the K-point. Here $\Theta(\boldsymbol{k})$ is shown for a k point on the E_{22} cutting line for both SWNTs. The difference between the type-I and type-II families can be understood from the position of the E_{11} or E_{22} cutting lines relative to the K-point.[22].

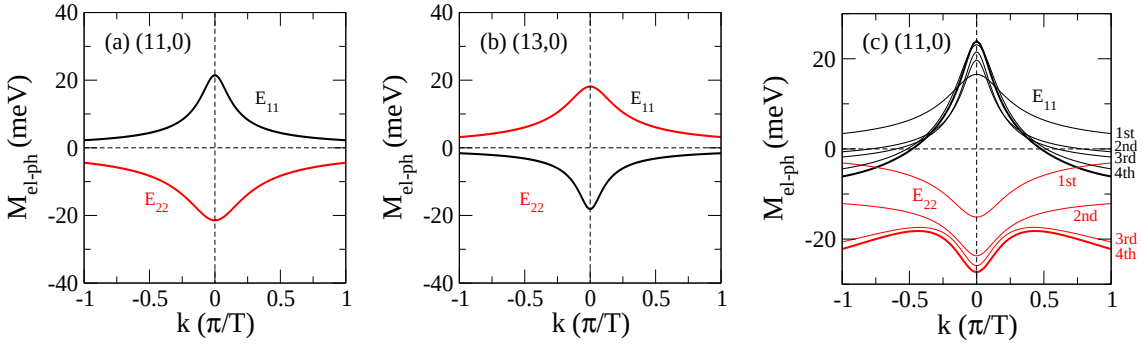

FIG. 5: (Color online) RBM electron-phonon matrix elements of (a) $(11,0)$ and (b) $(13,0)$ nanotubes calculated within the effective-mass theory using $g_{\rm off} = 6.4\,$eV. In panels (a) and (b), the matrix elements near $k = 0$ are comparable with the results in Fig. 2. Panel (c) shows the matrix elements of an $(11,0)$ nanotube calculated within the ETB model for interactions up to the fourth nearest-neighbors. The results including fourth nearest neighbors exactly reproduce the results in Fig. 2(a).

excited electron is basically a sum of conduction band c and valence band v electron-phonon matrix elements, which represent the electron and hole contributions, respectively,[20,26,28]

$$\begin{aligned} M_{\rm el-ph} &= M^{\rm c}_{\rm el-ph} - M^{\rm v}_{\rm el-ph} \\ &= \langle {\rm c}|H_{\rm el-ph}|{\rm c}\rangle - \langle {\rm v}|H_{\rm el-ph}|{\rm v}\rangle, \end{aligned} \tag{5}$$

where $H_{\rm el-ph}$ is the SWNT electron-phonon interaction Hamiltonian.

In Fig. 3, we plot the electron and hole components of $M_{\rm el-ph}$ in the ETB model as a function of the 1D wavevector k. If we compare the contributions from each component, we see that in the $(11,0)$ tube the electron (hole) component gives a larger contribution to $M_{\rm el-ph}$ at E_{11} (E_{22}). On the other hand, in the $(13,0)$ tube, the hole (electron) component gives a larger contribution to $M_{\rm el-ph}$ at E_{11} (E_{22}). We can analyze these results within an effective-mass theory.[27] Using the effective-mass theory, we can obtain a simple analytical expression explaining the sign of the SWNT electron-phonon matrix elements, which can then be compared with the ETB results.

In a nearest-neighbor effective-mass approximation, the RBM $H_{\rm el-ph}$ for an (n,m) SWNT with a chiral angle θ and diameter $d_{\rm t}$ can be written as[27]

$$H_{\rm el-ph} = \frac{2s_r}{d_{\rm t}} \begin{pmatrix} g_{\rm on} & -\frac{g_{\rm off}}{2}{\rm e}^{{\rm i}3\theta} \\ -\frac{g_{\rm off}}{2}{\rm e}^{-{\rm i}3\theta} & g_{\rm on} \end{pmatrix}, \tag{6}$$

where $g_{\rm on}$ ($g_{\rm off}$) is the on-site (off-site) coupling constant. Here $s_r = \sqrt{\hbar/2M\omega_{\rm RBM}}$ is the phonon amplitude for the RBM, where $\omega_{\rm RBM}$ is the phonon frequency and M is the total mass of the carbon atoms within the unit cell. To obtain $M_{\rm el-ph}$ in Eq. (5), we adopt the following two wavefunctions,

$$\Psi_{\rm c} = \frac{{\rm e}^{{\rm i}\boldsymbol{k}\cdot\boldsymbol{r}}}{\sqrt{2S}} \begin{pmatrix} {\rm e}^{-{\rm i}\Theta(\boldsymbol{k})/2} \\ {\rm e}^{+{\rm i}\Theta(\boldsymbol{k})/2} \end{pmatrix}, \Psi_{\rm v} = \frac{e^{i\boldsymbol{k}\cdot\boldsymbol{r}}}{\sqrt{2S}} \begin{pmatrix} {\rm e}^{-{\rm i}\Theta(\boldsymbol{k})/2} \\ -{\rm e}^{+{\rm i}\Theta(\boldsymbol{k})/2} \end{pmatrix}, \tag{7}$$

for conduction and valence states, respectively, which are suitable near the graphene K-point.[27] In Eq. (7), S is the surface area of graphene and $\Theta(\boldsymbol{k})$ is an angle at the K-point measured from a line perpendicular to the cutting lines (see Fig. 4).

By inserting the wavefunctions in Eq. (7) into Eq. (5), we obtain

$$+\langle {\rm c}|H_{\rm el-ph}|{\rm c}\rangle = \frac{s_r}{d_{\rm t}}\left(-g_{\rm off}\cos(\Theta(\boldsymbol{k})+3\theta)+2g_{\rm on}\right), \tag{8a}$$

$$-\langle {\rm v}|H_{\rm el-ph}|{\rm v}\rangle = \frac{s_r}{d_{\rm t}}\left(-g_{\rm off}\cos(\Theta(\boldsymbol{k})+3\theta)-2g_{\rm on}\right), \tag{8b}$$

and thus

$$M_{\rm el-ph} = \frac{s_r}{d_{\rm t}}\left(-2g_{\rm off}\cos(\Theta(\boldsymbol{k})+3\theta)\right). \tag{9}$$

From Eqs. (8a) and (8b), it is clear that the electron and hole contributions to $M_{\rm el-ph}$ are simply distinguished by the off-site and on-site interactions. These equations are thus qualitatively consistent with the results in Fig. 3. According

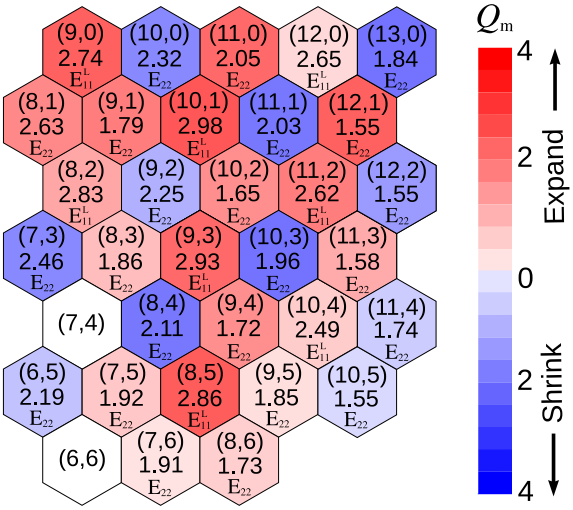

FIG. 6: (Color online) The lattice response of SWNTs with diameters in the range $0.7 - 1.1\,\mathrm{nm}$ is mapped onto the unrolled graphene lattice specifiying the tube chiralities (n, m). In this map Q_m is expressed in terms of $\sqrt{\hbar/2M\omega_{\mathrm{RBM}}}$. Red and blue colored hexagons denote the SWNTs whose vibrations start by increasing or decreasing their diameter, respectively. The laser excitation energies are selected within the range $1.5 - 3.0\,\mathrm{eV}$. For each (n, m) tube, the corresponding E_{ii} (in eV) found within this energy region is listed on each hexagon with the label E_{ii}. The calculated results for the $(7, 4)$ and $(6, 6)$ nanotubes are not shown in this figure because their $E_{11}^{\mathrm{L}} > 3.0\,\mathrm{eV}$ and the $(6, 6)$ tube gives a negligibly small Q_{m}.

to the density-functional calculation by Porezag *et al.*,[29] we adopt the off-site coupling constant $g_{\mathrm{off}} = 6.4\,\mathrm{eV}$ and the on-site coupling constant $g_{\mathrm{on}} = 17.0\,\mathrm{eV}$, which are calculated for the first nearest-neighbor carbon-carbon distance.[27] However, g_{on} has no effect on the electron-phonon matrix element since it vanishes in Eq. (9). The more accurate treatment for the effective-mass theory should consider the asymmetry between the valence bands and the conduction bands.[30]. Within the present model, we do not consider such an asymmetry since the chirality dependence of the electron-phonon matrix element can readily be described by the $\cos(\Theta(\boldsymbol{k}))$ term, which will give a positive or negative sign in front of g_{off}.

In Fig. 5, we then plot the matrix elements of Eq. (9) for the $(11, 0)$ and $(13, 0)$ nanotubes, where the on-site term (g_{on}) disappears and only the off-site term (g_{off}) contributes to $M_{\mathrm{el-ph}}$. It can be seen that the effective-mass theory (see Figs. 5(a) and (b)) nicely reproduces the ETB calculation results near $k_{ii} = 0$ (see Figs. 2(a) and (b)). However, the first nearest-neighbor effective-mass model cannot reproduce the ETB matrix element results at k far from $k_{ii} = 0$. We can see this since at E_{11} and E_{22} $M_{\mathrm{el-ph}}$ are almost symmetric around $M_{\mathrm{el-ph}} = 0$ in Figs. 5(a) and (b) but the $M_{\mathrm{el-ph}}$ are not symmetric in Figs. 2(a) and (b). In Fig. 5(c), we show $M_{\mathrm{el-ph}}$ for the $(11, 0)$ tube within the ETB model considering interactions up to the fourth nearest-neighbors. Based on this figure, we consider that the exact $M_{\mathrm{el-ph}}$ analytical expression at k far from the k_{ii} should take into account the longer-range electron-phonon interactions. Nevertheless, the first nearest-neighbor effective-mass theory has already given physical insight into the k-dependent $M_{\mathrm{el-ph}}$, and considering the approximation up to the fourth nearest-neigbors is sufficient to converge the $M_{\mathrm{el-ph}}$ values.

For the zigzag nanotubes, Eq. (9) also explains the dependence of $M_{\mathrm{el-ph}}$ on the cutting line (or $\boldsymbol{k}$) position. Let us take the examples in Fig. 4, in which we show the cutting lines for the $(11, 0)$ and $(13, 0)$ nanotubes. The E_{22} cutting line for the $(11, 0)$ ($(13, 0)$) tube is to the right (left) of the K-point, giving a positive (negative) $\cos(\Theta(\boldsymbol{k}))$ and thus a negative (positive) $M_{\mathrm{el-ph}}$ for the E_{22} transition. According to Eq. (2), the negative (positive) $M_{\mathrm{el-ph}}$ corresponds to the initial increase (decrease) of the tube diameter. In such a way, the chirality dependence of the coherent phonon amplitude is simply determined by the electron-phonon interaction. However, we should note that this simple rule does not work well for E_{33} and E_{44}, as can be seen in Fig. 1. For instance, the coherent phonon amplitude at E_{33} has the same sign as that at E_{22} although their cutting line positions are opposite to each other with respect to the K-point. The reason for the breakdown of this simple rule is that the cutting lines for E_{33} and E_{44} are far from the K-point so that the wavefunctions of Eq. (7) are no longer good approximations. In this case, the ETB wavefunctions are necessary for obtaining the coherent phonon amplitudes.

IV. GUIDE FOR EXPERIMENTALISTS

To consider the more general family behavior of the RBM coherent phonon amplitudes, we recalculate $Q_{\rm m}$ using the ETB program for 31 different SWNT chiralities with diameters of $0.7-1.1\,$nm and for photoexcitations at E_{ii} in the range $1.5-3.0\,$eV. The results are shown in Fig. 6. Note that in addition to the semiconducting SWNTs, we also give some results for metallic SWNTs. It is known that the density of states for E_{ii} in metallic SWNTs are split into the lower $E_{ii}^{\rm L}$ and higher $E_{ii}^{\rm H}$ branches, except for the armchair SWNTs.[16] Here we consider $Q_{\rm m}$ in metallic SWNTs only at $E_{11}^{\rm L}$. The cutting line for $E_{11}^{\rm L}$ is located to the right of the K-point. We can see in Fig. 6 that all the metallic SWNTs start vibrations by increasing their diameter at $E_{11}^{\rm L}$. The reason is the same as in type-II nanotubes, where the cutting lines for the E_{11} transitions are located to the right of the K-point, giving a negative $M_{\rm el-ph}$ (hence a positive $Q_{\rm m}$) as explained within the effective-mass theory. On the other hand, at $E_{11}^{\rm H}$, the nanotubes should start their coherent vibrations by decreasing their diameters. In the case of armchair nanotubes, for which $E_{11}^{\rm L}=E_{11}^{\rm H}$, we expect that no vibration should occur because the two contributions from $E_{11}^{\rm L}$ and $E_{11}^{\rm H}$ should cancel each other.

For semiconducting nanotubes, we see that most of the type-I (type-II) nanotubes start vibrating at E_{11} by decreasing (increasing) their diameters and at higher energies by increasing (decreasing) their diameters. In a few cases, e.g., $(7,6)$, $(9,5)$, and $(10,5)$ nanotubes, the deviation from this rule might come from the 3θ term in Eq. (9), especially for the near-armchair nanotubes where θ approaches $\pi/6$. As mentioned previously, we consider that in the case of armchair nanotubes, for example the $(6,6)$ nanotube, which is metallic, the coherent phonon amplitude becomes small because of the trigonal warping effect.[16] The exclusion of both excitonic effects and environmental effects may also be a reason for this deviation because the E_{ii} transition energies are also shifted to some extent.[24,25] Nevertheless, our results should stimulate further work by experimentalists to check for consistency with this prediction.

V. CONCLUSION

We found that the excitation and chirality dependence of the coherent phonon amplitudes in SWNTs originate mostly from the electron-phonon matrix elements. By examining typical tubes with chirality (n,m) of type-I and type-II SWNTs, respectively, we found that the nanotubes can start coherent RBM vibrations by either expanding or shrinking their diameters depending on the sign of the electron-phonon interaction in the SWNT system, where the $M_{\rm el-ph}$ values can either be positive or negative near the K-point. The magnitudes of the coherent phonon amplitudes are estimated to be proportional to $|M_{\rm el-ph}||M_{\rm op}|$. In the future, the effective mass theory can be extended to accommodate longer-range interactions so that the behavior of the coherent phonon amplitudes at the higher transitions, e.g. E_{33} and E_{44}, can be explained. In future studies incorporating excitonic effects, the exciton-photon and exciton-phonon matrix elements can be used to replace the electron-photon and electron-phonon matrix elements.

Acknowledgments

A.R.T.N. is supported by a Monbukagakusho scholarship. R.S. acknowledges MEXT Grant (No. 20241023). M.S.D. acknowledges NSF/DMR 10-04147. C.J.S. and G.D.S. acknowledge NSF (DMR-1105437 and OISE-0968405) and ONR-00075094. We are grateful to Prof. J. Kono of Rice University for fruitful discussions which stimulated this work. We thank Z. Nie *et al.* of the University of Electro-Communications Tokyo for sharing their experimental reports before publication.

[1] R. Saito, G. Dresselhaus, and M. S. Dresselhaus, *Physical Properties of Carbon Nanotubes* (Imperial College Press, London, 1998).
[2] M. S. Dresselhaus, *Carbon Nanotubes: Synthesis, Structure, Properties, and Applications* (Springer, New York, 2001).
[3] P. Harris, *Carbon Nanotubes and Related Structures: New Materials for the Twenty-First Century* (Cambridge University Press, Cambridge, England, 1999).
[4] J.-C. Charlier, X. Blase, and S. Roche, Rev. Mod. Phys. **79**, 677 (2007).
[5] V. Popov, New Journal of Physics, **6**, 17 (2004).
[6] A. Gambetta, C. Manzoni, E. Menna, M. Meneghetti, G. Cerullo, G. Lanzani, S. Tretiak, A. Piryatinski, A. Saxena, R. L. Martin, and A. R. Bishop, Nat. Phys. **2**, 515–520 (2006).
[7] Y. S Lim, K. J. Yee, J. H. Kim, E. H. Haroz, J. Shaver, J. Kono, S. K. Doorn, R. H. Hauge, and R. E. Smalley, Nano Lett. **6**, 2696–2700 (2006).
[8] K. Kato, K. Ishioka, M. Kitajima, J. Tang, R. Saito, and H. Petek, Nano Lett. **8**, 3102–3108 (2008).
[9] J.-H. Kim, K.-J. Han, N.-J. Kim, K.-J. Yee, Y.-S. Lim, G. D. Sanders, C. J. Stanton, L. G. Booshehri, E. H. Hároz, and J. Kono, Phys. Rev. Lett. **102**, 037402 (2009).
[10] K. Makino, A. Hirano, K. Shiraki, Y. Maeda, and M. Hase, Phys. Rev. B **80**, 245428 (2009).
[11] S. Kilina and S. Tretiak, Adv. Func. Mat. **17**, 3405 (2007).
[12] Y.-S. Lim, J.-G. Ahn, J.-H. Kim, K.-J. Yee, T. Joo, S.-H. Baik, E. H. Haroz, L. G. Booshehri, and J. Kono, ACS Nano **4**, 3222–3226 (2010).
[13] G. D. Sanders, C. J. Stanton, J.-H. Kim, K.-J. Yee, Y.-S. Lim, E. H. Hároz, L. G. Booshehri, J. Kono, and R. Saito, Phys. Rev. B **79**, 205434 (2009).
[14] Z. Nie and T. Kobayashi. *Private communications*.
[15] Keiko Kato, Katsuya Oguri, Atsushi Ishizawa, Hideki Gotoh, Hidetoshi Nakano, and Tetsuomi Sogawa, Appl. Phys. Lett. **97**, 121910 (2010).
[16] R. Saito, G. Dresselhaus, and M. S. Dresselhaus, Phys. Rev. B **61**, 2981–2990 (2000).
[17] A. V. Kuznetsov and C. J. Stanton, Phys. Rev. Lett. **73**, 3243–3246 (1994).
[18] Ge. G. Samsonidze, R. Saito, N. Kobayashi, A. Grüneis, J. Jiang, A. Jorio, S. G. Chou, G. Dresselhaus, and M. S. Dresselhaus, Appl. Phys. Lett. **85**, 5703 (2004).
[19] R.A. Jishi, L. Venkataraman, M.S. Dresselhaus, and G. Dresselhaus, Chem. Phys. Lett. **209**, 77–82 (1993).
[20] J. Jiang, R. Saito, Ge. G. Samsonidze, S. G. Chou, A. Jorio, G. Dresselhaus, and M. S. Dresselhaus, Phys. Rev. B **72**, 235408 (2005).
[21] J. Jiang, R. Saito, A. Grüneis, G. Dresselhaus, and M. S. Dresselhaus, Carbon **42**, 3169–3179 (2004).
[22] R. Saito, K. Sato, Y. Oyama, J. Jiang, Ge. G. Samsonidze, G. Dresselhaus, and M. S. Dresselhaus, Phys. Rev. B **72**, 153413 (2005).
[23] Ge. G. Samsonidze, R. Saito, A. Jorio, M. A. Pimenta, A. G. Souza Filho, A. Grüneis, G. Dresselhaus, and M. S. Dresselhaus, J. Nanoscience and Nanotech. **3**, 431–458 (2003).
[24] A. R. T. Nugraha, R. Saito, K. Sato, P. T. Araujo, A. Jorio, and M. S. Dresselhaus, Appl. Phys. Lett. **97**, 091905 (2010).
[25] J. Jiang, R. Saito, Ge. G. Samsonidze, A. Jorio, S. G. Chou, G. Dresselhaus, and M. S. Dresselhaus, Phys. Rev. B **75**, 035407 (2007).
[26] M. Machón, S. Reich, H. Telg, J. Maultzsch, P. Ordejón, and C. Thomsen, Phys. Rev. B **71**, 035416 (2005).
[27] Ken-ichi Sasaki, Riichiro Saito, Gene Dresselhaus, Mildred S. Dresselhaus, Hootan Farhat, and Jing Kong, Phys. Rev. B **78**, 235405 (2008).
[28] J. Jiang, R. Saito, A. Grüneis, S. G. Chou, Ge. G. Samsonidze, A. Jorio, G. Dresselhaus, and M. S. Dresselhaus, Phys. Rev. B **71**, 205420 (2005).
[29] D. Porezag, Th. Frauenheim, Th. Köhler, G. Seifert, and R. Kaschner, Phys. Rev. B **51**, 12947 (1995).
[30] H. Suzuura and T. Ando, Phys. Rev. B **65**, 235412 (2002).